AIAA 80-0330R

Inverse Transonic Wing Design Method

P. A. Henne*
Douglas Aircraft Company, Long Beach, Calif.

An inverse, transonic flow method for the design of three-dimensional wings has been developed. The flow method is based on a three-dimensional, finite-difference solution of the full-potential equation. The inverse scheme utilizes a Dirichlet boundary condition in conjunction with surface transpiration to affect geometry definition. Such a scheme has previously been utilized in a two-dimensional method. This paper summarizes an analogous development for three dimensions. Basic steps and underlying assumptions of the inverse scheme are described. Applications of the method to both simple and complicated design problems are discussed and advantages of the method are identified.

Nomenclature

$\mathcal{R}$ = wing aspect ratio
C_L = lift coefficient
C_P = pressure coefficient
i_w = wing section incidence angle
M = freestream Mach number
t/c = wing section maximum thickness-to-chord ratio
α = angle of attack
ΔC_D = incremental drag coefficient
η = semispan fraction
ρ/c = wing section leading edge radius-to-chord ratio

Introduction

THE design of efficient transonic airfoil sections and wing surfaces has been significantly aided by the development of computational transonic flow methods. Both two-[1-3] and three-dimensional[4-6] analysis methods have been developed to a reasonable level of accuracy and reliability for the evaluation of airfoil and wing characteristics.[1,2,7,8] Such analysis or direct-solution methods have become a standard feature in many contemporary wing development efforts[9-12] and provide an assessment of the flowfield that develops about a given geometry.

The development of analogous design or inverse computational transonic flow methods, that is, methods that define the geometry required to produce a given flowfield, has received less attention than the development of direct methods. Since inverse methods solve for the geometry, such methods eliminate much of the cut-and-try approach to geometry definition and complement direct methods in the development of airfoil and wing geometries. Several two-dimensional inverse methods based on the hodograph plane[13,14] have been developed but are restricted to shock-free flows. The two-dimensional inverse methods of Carlson[15] and Tranen,[16] on the other hand, allow flows with shock waves. The method of Tranen, in particular, provides a design capability with few restrictions and has proven to be quite effective for the design of transonic airfoil sections. The development of three-dimensional inverse methods has been limited to transonic small-disturbance theory approaches[17,18] and the "fictitious gas" scheme.[19] The small-disturbance theory approaches are subject to initial assumptions regarding the size of velocity perturbations, while the "fictitious gas" scheme attempts to develop shock-free, three-dimensional flow. The present method, summarized in this paper, does not follow either of these three-dimensional approaches, but is a three-dimensional, full-potential scheme analogous to the two-dimensional method of Tranen. Consequently, the present method is quite general and allows for three-dimensional shock systems.

Submitted Jan. 10, 1980; presented as Paper 80-0330 at the AIAA 18th Aerospace Sciences Meeting, Pasadena, Calif., Jan. 14-16, 1980; revision received May 30, 1980.

*Senior Engineer, Aerodynamics Group. Member AIAA.

Computation Method

Inverse Scheme

The present formulation assumes that an initial wing geometry exists and that small changes to the geometry are to be made. The changes are to be defined such that a specified pressure distribution is developed by the new geometry. The specified pressure distribution is known while the geometry displacement is unknown.

Figure 1 illustrates, in two dimensions, the fundamental technique used to relate the initial and new geometries. By definition, the new geometry is a particular streamline in the new flowfield. If the streamlines from the new flowfield are superimposed on the initial geometry, as indicated in Fig. 1, flow through the initial geometry surface is generated. Hence, the new geometry flowfield can be produced using the initial geometry and an appropriate normal flow or surface transpiration distribution. If this transpiration distribution is defined in conjunction with the initial geometry, then the new geometry can be developed from mass conservation considerations. By integrating the mass flux through the initial surface, the streamline defining the new geometry can be found. Thus, the problem is reduced to solving for the transpiration distribution.

The transpiration distribution is determined from a flow solution in which a Dirichlet-type boundary condition is imposed at the wing surface. A velocity potential is specified on the initial geometry, and the flowfield, including the transpiration distribution, is calculated. The specified velocity potential is derived from consideration of the surface tangent velocity. The specified velocity tangent to the new geometry is used to approximate the velocity tangent to the initial

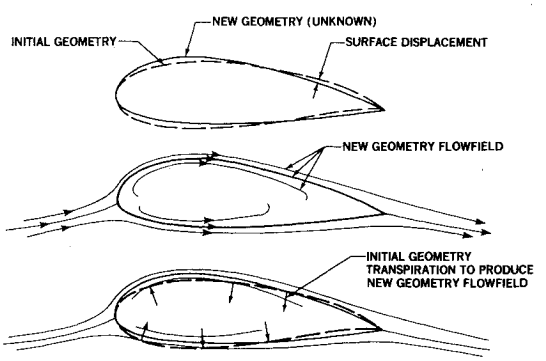

Fig. 1 Surface displacement generated by transpiration.

geometry in the new flowfield. This approximation is consistent with the assumption of small changes in the geometry and the corresponding small magnitude of the transpiration velocities.

The basic scheme is summarized as follows. The specified pressure distribution, converted to a velocity distribution, is integrated to define a specified velocity potential which is imposed on the initial geometry as a Dirichlet boundary condition. The resulting flow solution produces the desired transpiration distribution. The calculated normal flow is integrated to define the initial surface displacement required to obtain the new geometry. The essential ingredients of this scheme include the assumption of small changes, the application of a Dirichlet boundary condition, and the integration of the calculated transpiration.

The scheme just described includes a surface velocity integration to define a velocity potential. The integration is carried out in a streamwise direction at constant span stations. The determination of a unique surface potential normally would require an additional integration in the spanwise direction at some streamwise coordinate. In the present method, this integration is used to provide a trailing-edge thickness constraint. The spanwise integration is accomplished during the Dirichlet solution convergence and requires an iteration to maintain trailing-edge thickness. This technique provides a mathematically unique solution and a physically useful constraint. By constraining trailing-edge thickness, the development of re-entrant or excessively blunt trailing-edge geometries is avoided. Any loss in accuracy associated with distortion of the spanwise velocity components has been found to be negligible.

The scheme also includes a mass flux integration to determine the surface displacement. This mass flux integration is accomplished at constant span stations. Consistent with the assumption of small changes and the trailing-edge constraint, the spanwise component of velocity is neglected in the mass flux integration; the integration utilizes only the streamwise and vertical velocity components. The integration is initiated at the leading-edge "stagnation point" and proceeds downstream along each wing surface. The use of a mass flux control volume[16] conveniently defines the surface displacement. The basic steps of the present scheme, illustrated in Fig. 2, are summarized as:

1) Calculation of an initial, direct-flow solution for the initial geometry.

2) Modification of surface pressure distributions and corresponding surface velocity potential.

3) Calculation of a Dirichlet flow solution using a modified surface potential as a boundary condition.

4) Calculation of surface transpiration associated with the Dirichlet solution.

5) Integration of surface transpiration for surface displacement using mass conservation.

6) Addition of surface displacement to initial geometry to define new geometry.

7) Repeat step 1 for the new geometry.

The spanwise potential integration is accomplished by completing steps 3-5 during each potential iteration in the Dirichlet solution convergence.

As indicated above and in Fig. 2, the final step generates a direct-flow solution similar to the first step and provides closure for looping through multiple inverse cycles. For the present discussion, an inverse cycle is taken to be one pass through the steps listed above.

Basic Potential Flow Solution

The basic flow solution used in inverse cycle steps 1 and 3 is the three-dimensional transonic, full-potential flow solution of Jameson and Caughey.[4] This flow solution, known originally as FL022, is a nonconservative, finite-difference formulation utilizing a sheared, parabolic coordinate mapping of the wing surface. Since the same differencing scheme and relaxation procedure is used in both flow solution steps of the inverse cycle, the process is numerically consistent.

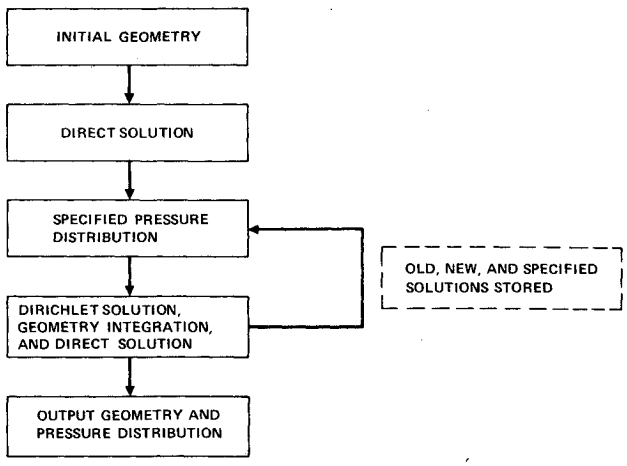

Fig. 2 Solution scheme for present method.

The original FL022 program has been updated with the following enhancements:

1) Accelerated iteration step[20]

2) Iterated Nash-Macdonald two-dimensional strip boundary-layer simulation[21]

3) Approximate fuselage volume and cross-flow effects

4) Multiple embedded meshes[22]

The accelerated iteration step and the multiple embedded meshes have been included to reduce computational costs. The multiple embedded meshes are based on original work by Boppe[22] and further development by the present author.

Viscous effects are included with an iterated two-dimensional strip boundary layer. The surface geometry with the initial boundary-layer displacement thickness added is modified in the inverse cycle. The initial boundary-layer displacement thickness is then removed to define the new surface. By using the same displacement thickness addition and subtraction, the trailing-edge thickness constraint is maintained.

The approximate fuselage effects provide a more realistic simulation of wing-body configurations than the original FL022 program. These effects include adjustments of the freestream Mach number and local wing section incidence and cause no significant increase in computational cost or complexity.

Implementation

The computational method has been implemented using an interactive computing environment. The computing system involves a Tektronix 4014-type graphics terminal in conjunction with batch and timeshare (TS/VS) on an IBM 3033 mainframe. A batch job is used to generate the initial direct solution. This solution is accessed via the 4014 terminal, and the user modifies the initial pressure distribution as desired. On-line graphics capabilities to aid the user include two- and three-dimensional pressure distributions, airfoil section comparisons, and planform view isobar patterns. A batch job is then submitted from the terminal to solve for the Dirichlet flowfield, perform the necessary normal flow integration and geometry modification, and solve for a direct flowfield on the new geometry. The final direct solution serves two purposes. First, it defines the match obtained between the specified pressure distribution and the pressure distribution actually obtained with the new geometry. Second, it provides the initial solution for additional cycles if a more accurate match of the specified and new pressures is required or if a different pressure distribution is desired. An inverse cycle can be completed very quickly; hence, capability for rapid development of the wing geometry is provided.

The computing cost of the inverse has been found to be less than expected. Originally, the cost of an inverse program cycle was predicted to be equivalent to the cost of two direct-flow solutions, since twice the computational work was predicted. However, the inverse potential iterations and the subsequent direct-potential iterations converge rapidly with no apparent loss in accuracy if the solution is started from the previous potential field. As shown in Fig. 3, recent experience indicates the computational cost of an inverse cycle (inverse plus direct-potential iterations) is usually less than a single direct solution started with a zero-potential field.

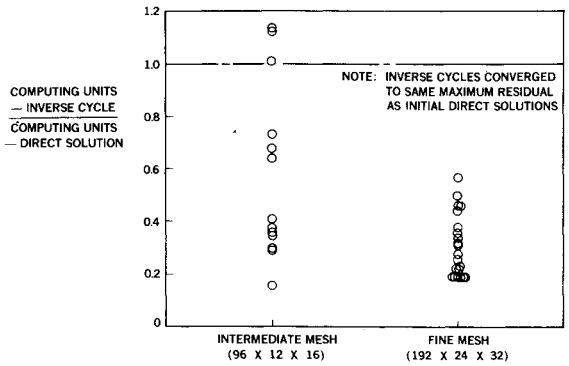

Fig. 3 Inverse cycle computing cost compared to initial direct-solution computing cost.

Applications

Check Cases

Results from two check cases are presented to substantiate the accuracy of the inverse program. Both check cases were computed in an intermediate mesh ($96 \times 12 \times 16$) and demonstrate the ability of the program to recover the original wing geometry subsequent to an initial modification.

The initial geometry for the first case is an untwisted rectangular wing with an aspect ratio of 10 and an NACA 0012 airfoil section. The flow conditions for this case are 0.8 Mach number and 0 deg angle of attack. The wing was modified by specifying a change in the upper surface pressure distribution near the middle of the wing. The results shown in Fig. 4 include the original, specified, and new pressure distributions and the original and new wing sections for one inverse cycle. As shown in Fig. 4, the pressure coefficient upstream of the shock on only the upper surface was made more negative at 39% semispan. This bump in the wing upper surface pressure distribution was washed out inboard and

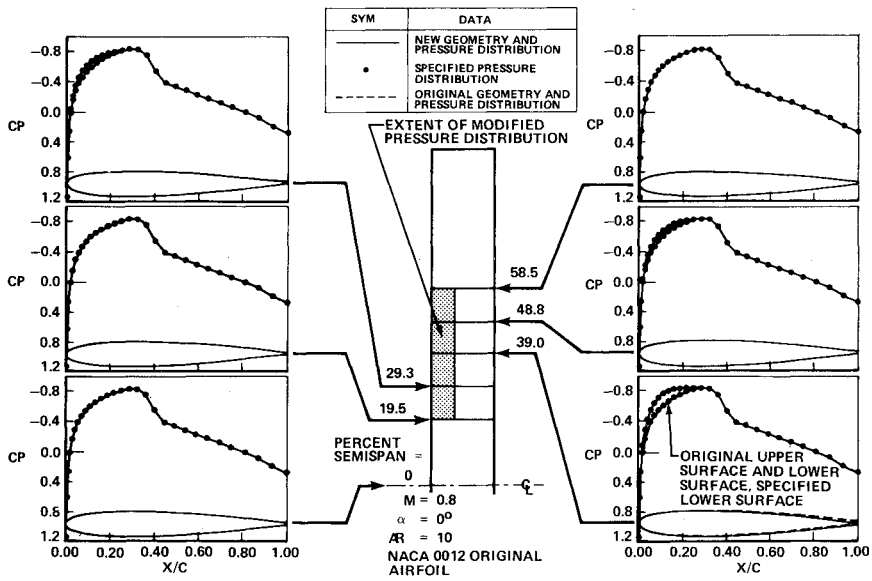

Fig. 4 Modification of symmetric straight wing upper surface pressure distribution.

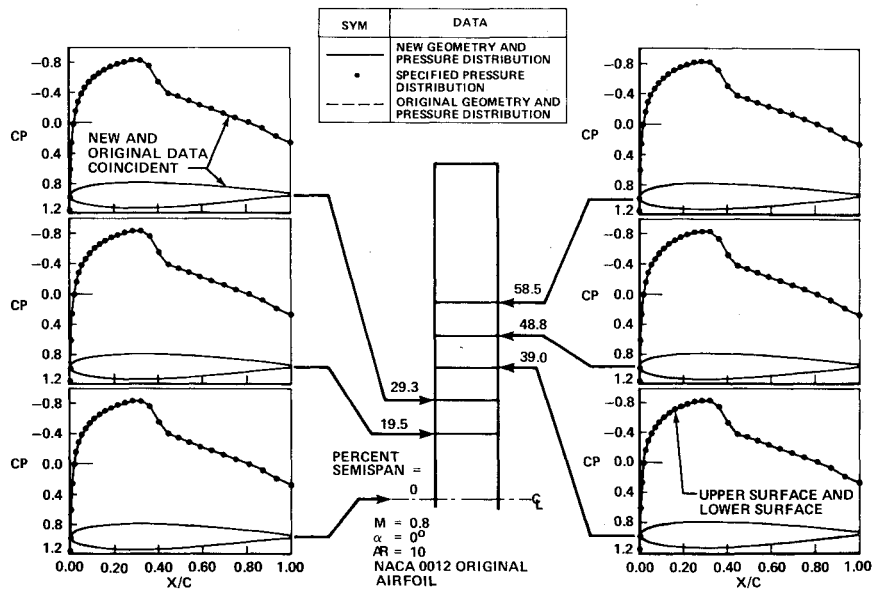

Fig. 5 Recovery of symmetric straight wing geometry.

outboard in two span stations. The agreement between the specified and new pressure distributions is quite good. The modified geometry and corresponding wing pressure distributions were then used as the initial solution for additional inverse cycles. In these cycles, the original pressure distribution was respecified in an attempt to recover the old geometry. The results shown in Fig. 5 indicate that the old geometry was accurately recovered in two inverse cycles. The new, specified, and original pressure distributions and the new and original geometries are identical for all practical purposes.

The spanwise distribution of maximum thickness-to-chord ratio, wing-section incidence, and section lift coefficient for the original, modified, and recovered geometries are illustrated in Fig. 6. An induced geometry effect is noted beyond the spanwise extent of the pressure distribution changes. This interesting effect is a natural consequence of an inverse solution and can be explained by first considering a direct solution. It is recognized that geometry changes in a direct solution induce changes in the pressure distribution beyond the extent of the geometry changes. Likewise, it is reasonable to expect that pressure distribution changes in an inverse solution induce changes in the geometry beyond the extent of the pressure distribution changes. The recovered geometry characteristics indicated in Fig. 6 are essentially the same as the original geometry.

The initial geometry for the second case is a simple, untwisted swept wing with a constant NACA 64_1212 normal airfoil section. The aspect ratio is 6.0 and the quarter chord sweep is approximately 35 deg. The flow conditions for the solution are 0.85 Mach number and 2.0 deg angle of attack. This case addresses the classical transonic root design problem

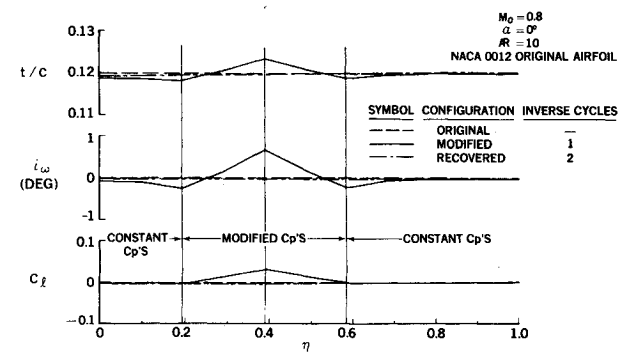

Fig. 6 Spanwise distribution of airfoil thickness ratio, section incidence, and section C_l for symmetric straight wing case.

for a swept wing. The inboard pressure distribution was modified, to reduce the characteristic unsweeping of the isobars near the root. The specified pressure distributions were defined with the same section lift coefficient as the original pressure distributions, but the airfoil loading was increased near the leading edge and decreased near the trailing edge. Figure 7 presents a comparison of the original, specified, and new pressure distributions and the original and new wing section geometries. Three inverse cycles were used to generate the new geometry. A substantial change is noted in the inboard wing section geometries.

The modified geometry and corresponding flow solution were used as an initial solution for recovering the original wing geometry. The recovery results calculated after five inverse cycles are presented in Fig. 8. The original wing geometry has been well recovered with only a small discrepancy, not apparent to the scale of Fig. 8, near the leading edge of the root airfoil. Additional cycles could be used to reduce this discrepancy. The spanwise distribution of maximum thickness-to-chord ratio, section incidence, and leading-edge radius-to-chord ratio is presented in Fig. 9 for the original, modified, and recovered geometries. Substantial changes are noted in the inboard area for the modified geometry. The root leading-edge discrepancy in the recovered geometry is apparent only in the leading-edge radius ratio. The thickness ratio and section incidence have been well recovered all across the span.

These check cases indicate that the inverse program is quite accurate in obtaining a specified pressure distribution. The program is also consistent in that a geometry can be modified and subsequently recovered.

Sample Cases

Numerous additional cases have been addressed with the inverse program using either intermediate or fine mesh solutions. Two of these cases are presented to indicate the utility and broad capabilities of the method. The first case utilizes the same swept wing geometry as described previously, but was calculated with a fine mesh ($192 \times 24 \times 32$) for better shock wave resolution. The second case is a modification study of a high-aspect-ratio supercritical wing design. Since shock wave resolution was not an important consideration for the second case, an intermediate mesh was used to reduce computational costs.

The objective of the first case was to increase the sweep of the shock near the root of a swept wing at transonic conditions. The isobar pattern for the initial fine mesh direct solution for the simple swept wing described in the section on check cases is presented in Fig. 10. Considerable shock un-

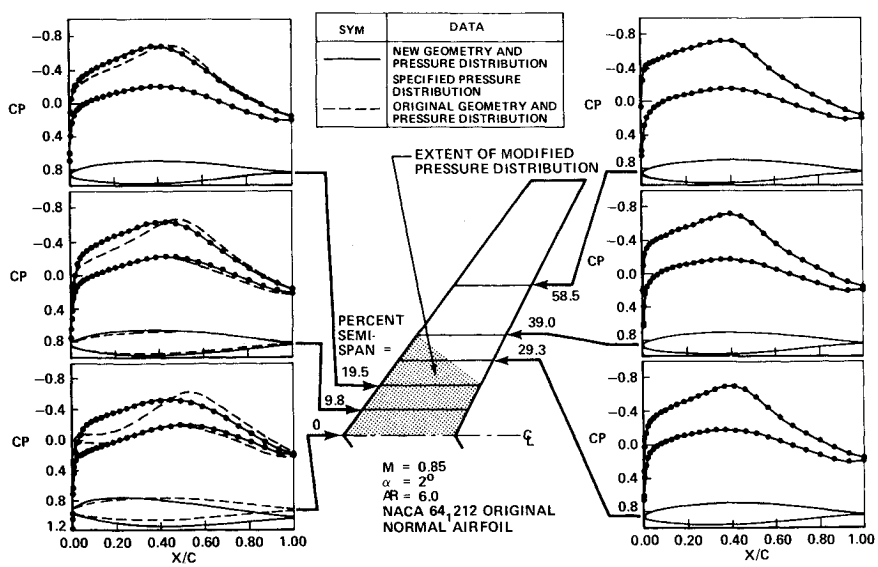

Fig. 7 Modification of cambered swept wing inboard pressure distribution.

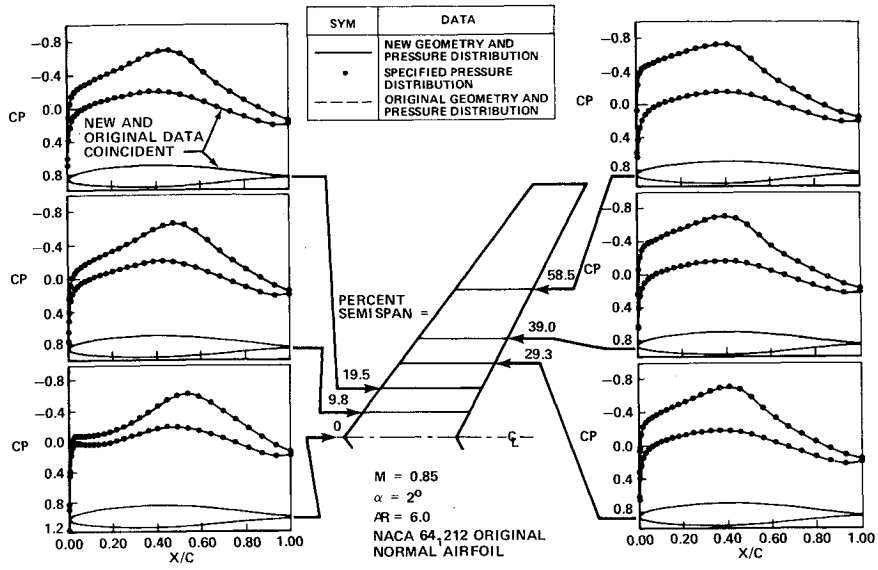

Fig. 8 Recovery of cambered swept wing geometry.

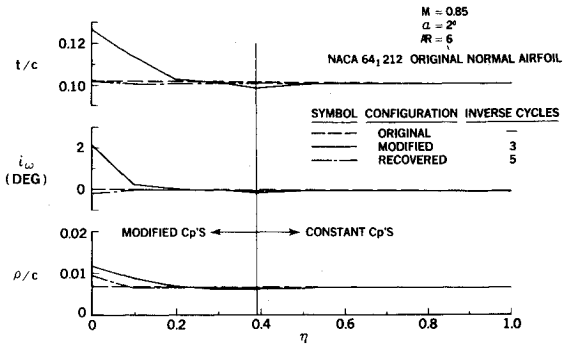

Fig. 9 Spanwise distribution of airfoil thickness ratio, section incidence, and leading-edge radius ratio for cambered swept wing case.

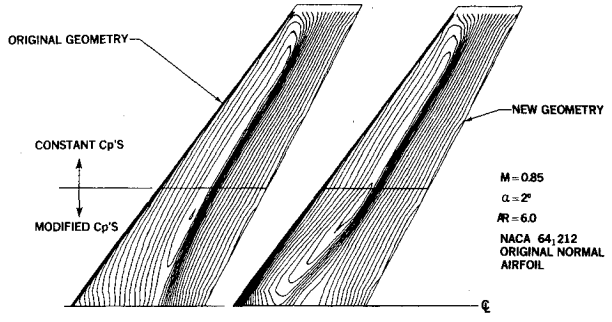

Fig. 10 Comparison of upper surface isobars for cambered swept wing inboard shock modification.

sweeping is evident inboard. Also presented in Fig. 10 is the isobar pattern for a geometry modification after seven inverse cycles. The inboard shock sweep is substantially increased with this new geometry. The shock near the root has been repositioned forward about 30% chord. The pressure distributions were specified to maintain section lift coefficient and hold the C_P ahead of the shock at nearly the same value. The original, specified, and new pressure distributions and the original and new geometries are presented in Fig. 11. Large changes in the wing section geometries have been affected. Since the shock sweep has been increased significantly, the Mach number normal to the shock has been reduced. Compressibility drag associated with this shock wave should be reduced for the modified geometry.

The objective of the second case was to take an existing high-performance, supercritical wing design and further improve its capabilities. The following four objectives were sought:

1) Reduced compressibility drag creep
2) More positive pitching moment due to the wing
3) Increased inboard rear spar depth
4) Decreased wing lower surface velocities near the engine pylon leading edge.

These objectives were accomplished by specifying pressure distributions in an intermediate mesh solution at the design Mach number, but a relatively low C_L. The low C_L condition was used so that the upper surface pressure distribution was essentially a "sonic plateau" and no strong shock waves were present. This condition differs from the previous case in which a relatively strong shock was physically repositioned. Pressure distribution modifications were specified to reduce the inboard upper surface suction peaks (objective 1), to increase the inboard lower surface velocities in the aft portion of the wing (objectives 2 and 3), and to decrease the velocities near the pylon leading edge (objective 4). Six inverse cycles were used to develop the geometry modification. The results shown in Fig. 12 include the original, specified, and new pressure distributions and the original and new geometries. Again, large changes have been made to the inboard wing section geometry.

Fine mesh direct solutions for the original and for the modified geometries were calculated to assess the success in achieving the four objectives. A comparison of fine mesh calculated isobars and section pressure distributions at the design condition is presented in Fig. 13. For the new geometry, the inboard upper surface suction peaks are reduced, the aft loading inboard is reduced, and the velocities near the pylon leading edge (32% semispan) have been lowered. The calculated shock wave position is essentially unchanged. The results of these calculations indicate that the drag creep was reduced by $\Delta C_D = 0.0003$ at cruise, pitching moment was made more positive by 0.015, the root rear spar depth was increased more than 50%, and lower surface velocities near the pylon leading edge were significantly reduced. Hence, all four objectives were achieved.

Summary and Conclusions

As shown in Fig. 14, the development of the present method completes the set of four methods available for the design and development of efficient wing contours for transonic conditions. The four methods identified are mathematically consistent; all are full-potential, nonconservative formulations. The direct and inverse methods utilize the same differencing scheme. Likewise, two- and three-dimensional inverse methods are based on analogous schemes.

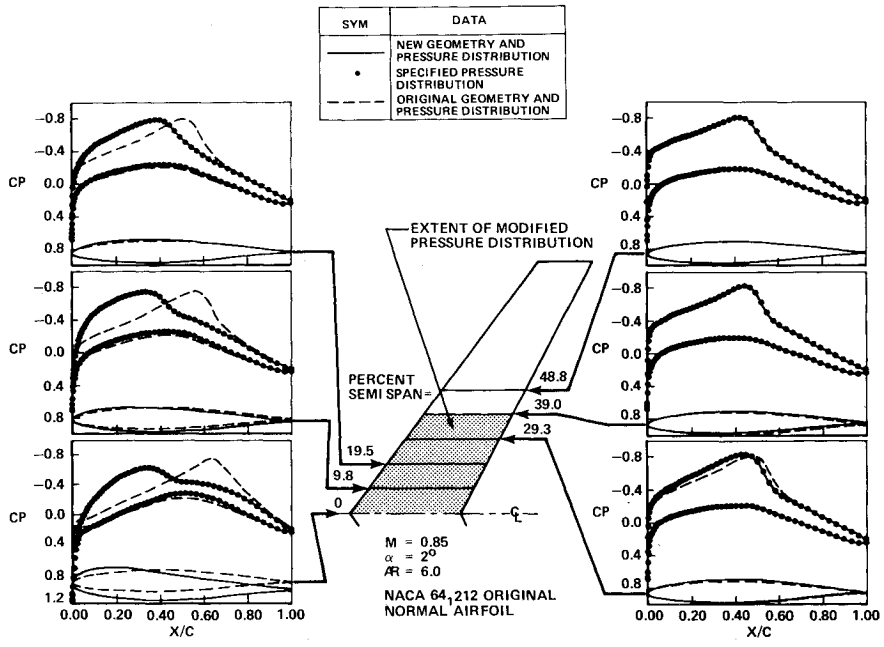

Fig. 11 Modification of cambered swept wing inboard shock development.

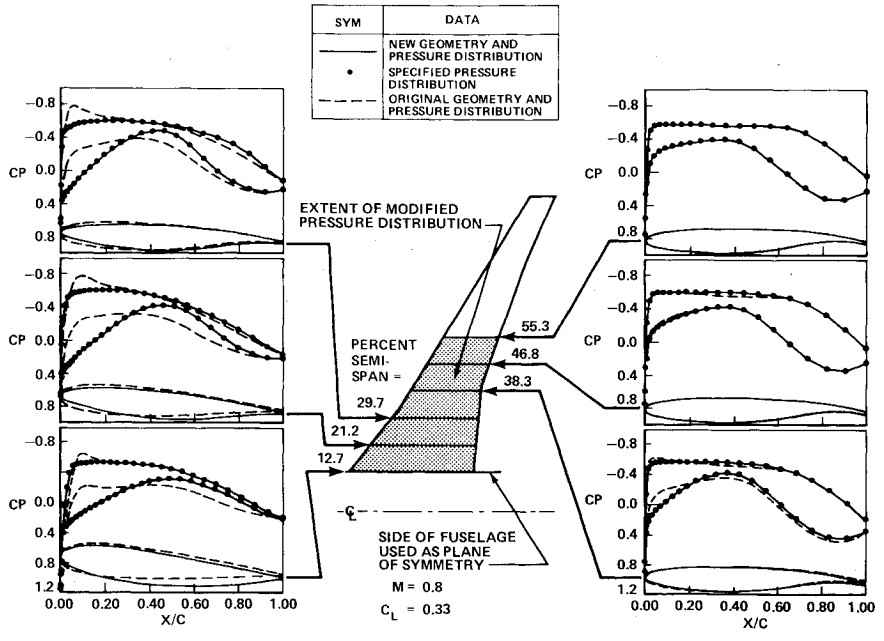

Fig. 12 Modification of supercritical swept wing inboard pressure distribution.

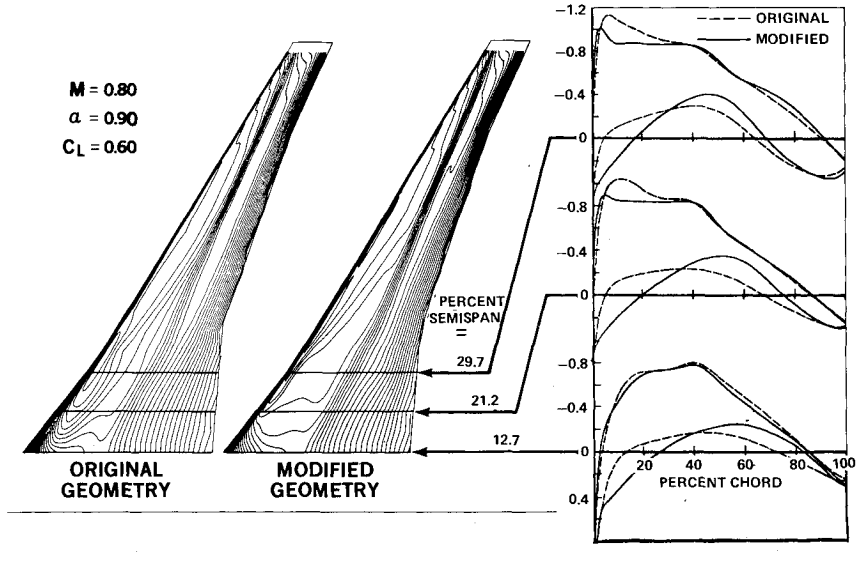

Fig. 13 Comparison of fine mesh isobars and chordwise pressure distributions for original and modified supercritical swept wing geometries.

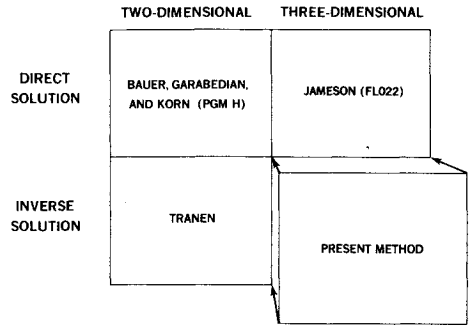

Fig. 14 Set of four computational transonic flow methods.

The applications of the inverse program indicate a significant advancement in transonic wing aerodynamic design capability.

Specific conclusions include the following:

1) Surface transpiration in conjunction with a Dirichlet boundary condition has been successfully used to develop an inverse, three-dimensional, full-potential, transonic flow method.

2) The method has been found to be quite accurate in obtaining a specified pressure distribution and consistent in the modification and subsequent recovery of initial geometry.

3) Convergence of the potential solution has been found to be rapid and associated computing costs are reasonable.

4) Implementation of the method in an interactive computing environment provides for rapid development of wing geometries.

References

[1] Bauer, F., Garabedian, P., Korn, D., and Jameson, A., *Supercritical Wing Sections II, Lecture Notes in Economics and Mathematical Systems,* Vol. 108, Springer-Verlag, New York, 1975.

[2] Melnik, R.E., Chow, R., and Mead, H.R., "Theory of Viscous Transonic Flow Over Airfoils at High Reynolds Number," AIAA Paper 77-680, Albuquerque, N. Mex. June 1977.

[3] Jameson, A., "Acceleration of Transonic Potential Flow Calculations on Arbitrary Meshes by the Multiple Grid Method," AIAA Paper 79-1458, Williamsburg, Va., July 1979.

[4] Jameson, A. and Caughey, D.A., "Numerical Calculation of the Transonic Flow Past a Swept Wing," New York University ERDA Rept. C00 3077-140, 1977.

[5] Jameson, A. and Caughey, D.A., "A Finite Volume Method for Transonic Potential Flow Calculations," AIAA Paper 77-635, Albuquerque, N. Mex., June 1977.

[6] Caughey, D.A. and Jameson, A., "Recent Progress in Finite-Volume Calculations for Wing-Fuselage Combinations," AIAA Paper 79-1513, Williamsburg, Va., July 1979.

[7] Henne, P.A. and Hicks, R.M., "Wing Analysis Using a Transonic Potential Flow Computational Method," NASA TM-78464, July 1978.

[8] DaCosta, A.L., "Application of Computational Aerodynamics Methods to the Design and Analysis of Transonic Aircraft," ICAS Paper B2-01, Lisbon, Portugal, Sept. 1978.

[9] Hicks, R.M. and Henne, P.A., "Wing Design by Numerical Optimization," AIAA Paper 77-1247, Seattle, Wash., Aug. 1977.

[10] Haney, H.P., Johnson, R.R., and Hicks, R.M., "Computational Optimization and Wind Tunnel Test of Transonic Wing Designs," AIAA Paper 79-0080, New Orleans, La., Jan. 1979.

[11] Lores, M.E., Smith, P.R., and Hicks, R.M., "Supercritical Wing Design Using Numerical Optimization and Comparisons with Experiment," AIAA Paper 79-0065, New Orleans, La., Jan. 1979.

[12] Lynch, F.T., "Recent Applications of Advanced Computational Methods in the Aerodynamic Design of Transport Aircraft Configurations," Douglas Paper No. 6639, Lisbon, Portugal, Sept. 1978.

[13] Nieuwland, G.Y., "Transonic Potential Flow Around a Family of Quasi-Elliptical Aerofoil Sections," N.L.R. Tech. Rept. T.172, 1967.

[14] Bauer, F., Garabedian, P., and Korn, D., *Supercritical Wing Sections, Lecture Notes in Economics and Mathematical Systems,* Vol. 66, Springer-Verlag, New York, 1972.

[15] Carlson, L.A., "Transonic Airfoil Design Using Cartesian Coordinates," NASA CR-2578, 1976.

[16] Tranen, T.L., "A Rapid Computer-Aided Transonic Airfoil Design Method," AIAA Paper 74-501, Palo Alto, Calif., June 1974.

[17] Shankar, V., Malmuth, N.D., and Cole, J.D., "Computational Transonic Design Procedure for Three-Dimensional Wings and Wing-Body Combinations," AIAA Paper 79-0344, New Orleans, La., 1979.

[18] Haines, A.B., "Computer-Aided Design: Aerodynamics," *Aeronautical Journal,* Vol. 83 March 1979, pp. 81-91.

[19] Fung, H.Y., Sobieczby, H., and Seebass, R., "Numerical Aspects of the Design of Shock-Free Wings and Wing-Body Combinations," AIAA Paper 79-1557, Williamsburg, Va., July 1979.

[20] Caughey, D.A. and Jameson, A., "Accelerated Iterative Calculation of Transonic Nacelle Flowfields," AIAA Paper 76-100, Washington, D.C., Jan. 1976.

[21] Nash, J.F. and Macdonald, A.G.J., "The Calculation of Momentum Thickness in a Turbulent Boundary Layer at Mach Numbers up to Unity," ARC CP No. 963, 1967.

[22] Boppe, C.W., "Calculation of Transonic Wing Flows by Grid Embedding," AIAA Paper 77-207, Los Angeles, Calif., Jan. 1977.